

# Computational Failure Modeling of Lower Extremities

**Reuben H. Kraft and Megan L. Lynch**

U.S. Army Research Laboratory

ATTN: RDRL-WMP-B

Aberdeen Proving Ground, Maryland 21005

United States of America

**Edward W. Vogel III**

Oak Ridge Institute for Science and Education

[reuben.h.kraft.civ@mail.mil](mailto:reuben.h.kraft.civ@mail.mil)

## **ABSTRACT**

*Underbelly blasts to vehicles from improvised explosives cause severe injuries to the lower extremities, including bone fracture, ligament tear, and muscle rupture. While these injuries may seem well-defined through medical imaging, the process of injury and the effects of vehicle system design to protection are still unclear. In this paper, efforts focused on developing a finite element model of the lower extremities undergoing high strain rate blast-induced deformation leading to injury will be discussed. A hierarchical approach is taken. The process of high strain rate direct axial loading that leads to bone fracture and fragmentation is investigated.*

## **1.0 INTRODUCTION**

Improvised explosive devices (IEDs) pose a major threat to the Warfighter and are oftentimes hidden along roads and detonated underneath trucks or tanks. The explosion beneath the vehicle is commonly referred to as an underbelly blast event. It has been reported that 8,159 IED incidents occurred in Afghanistan in 2009, which was an increase from 3,867 and 2,677 which were reported in 2008 and 2007, respectively [1]. During an underbelly blast, the lower extremities may experience accelerations in the range of 155 to 217 G [2] (note that civilian car traffic accidents are in the range of 5 to 35 G [3]). In order to design enhanced protective systems for this particular threat, the process of the insult to the injury must be well understood to discover the critical balance between performance and protection. Computational modeling offers a powerful tool to explore the insult-to-injury process with high-resolution.

When studying a complex dynamic process such as this, it is important to understand the length and time scales with the event. In vehicular mine blasts, multiple types of blast effects are present including primary, secondary and tertiary blast [4]. However, many of the musculoskeletal injuries are currently believed to be caused by tertiary blast effects (for example, from displacement of air by the explosion that creates a blast wind that can throw victims against solid objects) [5]. During an underbelly blast event, within 0.5 ms of the initiation of the explosion, a shock wave hits the bottom plate of the vehicle and causes a rapid rise in pressure. This pressure results in local acceleration and subsequent deformations of the plate which apply significant axial loads to the soldier and their legs [6]. As the blast wave reflects under the vehicle, a pressure force acts on

the bottom of the vehicle and causes it to lift off the ground. The acceleration of the vehicle and the collisions that follow are also a significant source of injury, especially if the soldier is not properly restrained. The body is subjected to both the local effects (caused by shock and high rate deformation of the vehicle) and global effects (vehicle motion over time) as a result of the mine detonation process. The nature of lower extremity injuries that occur during a mine blast may be broadly distinguished, similar to Kuppa *et al.* [7], as:

- Knee-thigh-hip complex fractures
- Knee ligament tears
- Tibia plateau/condyle fractures
- Tibia/fibula shaft fractures
- Calcaneus, ankle, and midfoot fractures
- Malleolar fractures and ligament tears and ruptures.

Some of the understanding for injuries experienced within the underbelly blast environment can be obtained from the civilian vehicle crash environment. For example, fractures of the ankle and lower foot which are predominant within the military environment, have already been studied in the past. Manning *et al.* [8] report that calcaneal, talar, midfoot and various other ankle fractures have been attributed to the mechanism of axial loading through the plantar surface of the foot. While these injuries might be expected from axial loading, Crandall *et al.* [9] demonstrated that even malleolar fractures can occur from pure dynamic axial loading of the leg. Begemen and Paravasthu [10] also conducted experimental impact tests where unembalmed cadaveric legs were subjected to a uniaxial plantar surface load along the axis of the tibia. Pilon<sup>1</sup> and calcaneal fractures were observed with the average failure tibial axial force of 7590 N. Kuppa [7] offers a useful review of calcaneus, talus, ankle and midfoot fracture research, most of which was conducted on postmortem human subjects. While this past research highlights some common features with military blast injuries, it is important to note that the rate of loading to the lower extremities may be 10 – 100 times greater than civilian vehicular crashes. Thus, there is a strong possibility that different injury mechanisms may be activated during these events and new or enhanced injury criteria may be required.

There have been attempts to computationally model underbelly blast effects in the lower extremities. Nilakantan and Tabiei [2] attempted to assess injury by measuring tibia compressive loads following an underbelly blast event using finite element analysis of a HYBRID III human surrogate, but the model fails to capture specific injury mechanisms such as bone fracture and ligament and joint failure. They make clear that more advanced and biofidelic lower extremity finite element models are needed. Many lower extremity studies employ a combined experimental and simulation-based approach. For example, Manseau and Keown [11] compared a physical lower leg model and a computer model in the development of enhanced injury assessment methods, with a focus on the ankle complex and its connections to the tibia. Once again, the models that were developed were not of high biological fidelity and could only offer some information.

In this paper we develop a series of numerical models in an effort to understand dynamic failure of the lower extremities subjected to underbelly blast loading. The lower legs will be modeled using three-dimensional, Lagrangian finite element analysis [12]. One long-term objective of this research is to have the capability to provide uncertainty quantification and robust validation for the lower extremity model. For this reason we adopt the method of Thacker *et al.* [13] who used a hierarchical methodology for creating a numerical model of the spine. Section 2.0 describes the computational methodology and results for three distinct finite element models: a component level tibia model (2.2), a lower leg assembly model (2.3) and a full lower extremity system model (2.4). Conclusions and future work will then be presented in Section 3.0.

---

<sup>1</sup>A pilon fracture occurs when one bone is driven into another bone with extreme force that may lead to comminuted fracture. The break occurs across the entire bone and into the ankle joint. It results from a high-energy loading injury from the foot up into the bone.

## 2.0 COMPUTATIONAL METHODOLOGY AND RESULTS

### 2.1 Model Hierarchy

Thacker *et al.* [13] provide a useful hierarchical verification and validation scheme that decomposes a system level model into components, subassemblies and assemblies. Within the validation and verification process, the process should start at smaller length scales, such as the components, and progress to the last stage of system level models. This approach requires simulations and experiments to be conducted at each level. While the current research effort adopts the approach, we note that this effort is a work-in-progress and is still in an early stage of building such a infrastructure and research team to support both the experimental and numerical models at the multiple length scales required. Nevertheless, we begin to define the subdivisions for the lower extremities for this effort and to also help pave the way for future work. The lower extremity system is partitioned into components (ligaments, muscles, bone, skin), subassemblies (joints), assemblies (motion segments consisting of muscles, joints, bones) and system level (whole leg) models as depicted in Figure 1.

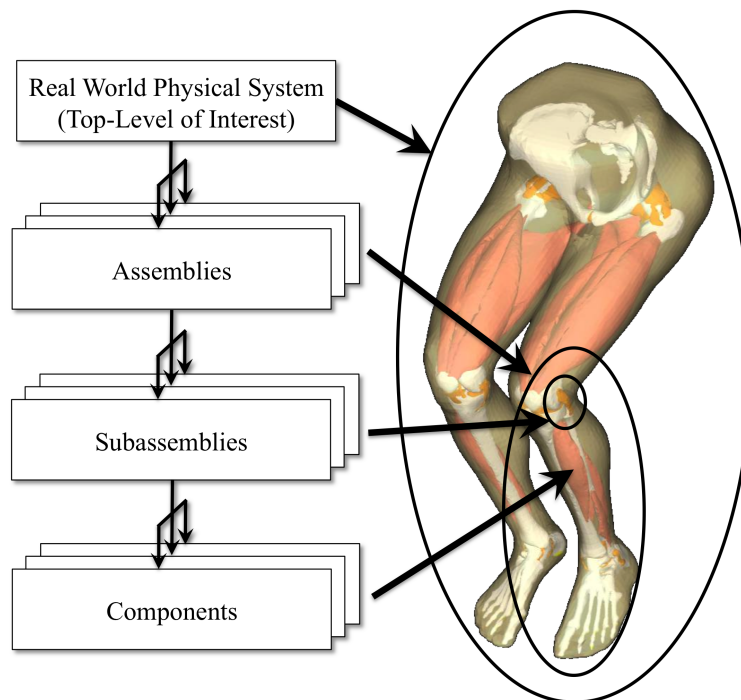


Figure 1: Validation hierarchy for the lower extremities based on the method of Thacker *et al.* [13]. The system is decomposed into components, subassemblies, assemblies and system level models.

### 2.2 Component Level Modeling of Bone Fracture and Failure Mechanics

Within the hierarchical modeling strategy, the component is the smallest length scale considered. Here we consider only one component of many, the tibia bone. The interest in bone from a biomechanical perspective is largely motivated by the fact that bones fracture, and that different fracture mechanisms may be activated during a blast event, as described in Section 1.0. An improved understanding of the mechanisms underlying

bone fracture and the ability to predict when fractures will occur may help in the development of new strategies for fracture prevention and treatment. Bones can fail in a variety of ways. If a bone is loaded monotonically to a stress level that exceeds the failure or ultimate stress of the bone tissue, then fracture will occur. This type of failure can occur with trauma or impact. Bone can also fail at stress levels well below the yield stress through the growth of preexisting cracks, but this will not be discussed here.

In this component level study the tibia is segmented into two parts representing cortical and trabecular bone, with the properties listed in Table 1. The medullary cavity and other anatomy is not represented here as the trabecular bone component fills the entire cortical shell. Axial displacement was applied to the proximal (top) surface of the tibia as the distal (bottom) surface remained fixed.

There are various approaches to modeling bone fracture numerically including element deletion, the cohesive zone approach, eXtended Finite Element Modeling (XFEM) and peridynamics. As Song *et al.* [14] point out, the element deletion method is one of the simplest methods for fracture simulation within the framework of the conventional FEM since there is no need to explicitly represent strong discontinuities in displacement fields (since fracture is modeled by a set of deleted elements). The element deletion method is used for this research due to simplicity. Once “broken” the elements have zero stress *i.e.* zero material resistance, which is implemented by using a constitutive equation in which the stress tends to zero for sufficiently large strain; an example of such a stress-strain law is shown in Figure 2. Similar to other numerical failure modeling techniques, element deletion introduces additional length and time scales into the simulations - some linked with physically-based parameters such as material toughness, and some numerical, such as the softening response. Therefore, effects of constitutive law parameters and strain rate on the resulting fracture morphology were investigated.

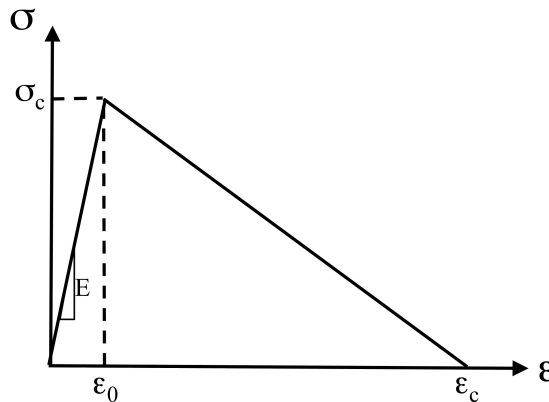


Figure 2: Schematic showing the elastic-fracture constitutive model used to capture fracture. First there is a linear elastic response until a critical stress,  $\sigma_c$ , is reached within the element, then linear stress softening occurs until the element critical crack opening stretch,  $\epsilon_c$ , is reached.

**2.2.1 Effect of Critical Crack Opening Stretch**

One of the crucial points in using the element deletion method is the scaling of the constitutive equation. Unless the constitutive equation is adjusted to reflect element size, the released energy due to deleting an element depends on the element size, which causes mesh dependency. To reduce mesh dependency, the softening curve slope should be scaled so that fracture energy is independent of the element size. The energy dissipation in an element with this stress-strain law is then equated to the surface energy of a crack passing through the element parallel to the sides by modifying the stress-strain law. This energy consistency renders solutions relatively

mesh size independent. To obtain energy equivalence in two dimensional problems for the stress-strain law shown in Figure 2, the upper strain limit  $\epsilon_c$  (referred to as the critical crack opening stretch) is scaled so that:

$$G_c h^e = \frac{1}{2} E \epsilon_0 \epsilon_c A^e \quad (1)$$

where  $G_c$  is the fracture energy,  $h_e$  is the characteristic dimension (the length of a side for a element) and  $A^e$  is the area of the element with unit thickness assumed. Recall the relationship given by elastic fracture mechanics between the mode-I stress intensity factor,  $K_I$ , and the energy release rate of the material,  $G_c$  given by  $K_I^2 = E' G_c$  where  $E' = E$  for plain stress or  $E' = E/(1 - \nu^2)$  for plain strain. Ural *et al.* [15] reports that bone has a fracture toughness of 7-10 MPa $\sqrt{m}$ . Therefore, in plane stress with  $E = 19$  GPa and  $K_{IC} = 7$  MPa $\sqrt{m}$ ,  $G_c = 2578$  J/m<sup>2</sup>. The characteristic dimension, or length of a side of an element is 0.001 m for the tibia finite element mesh. In order to calculate an estimate for the upper strain limit the tibia mesh is assumed to consist of equilateral tetrahedrons in which the area of the elements is uniform and is given by  $A_e = \frac{1}{2}(0.001)^2$  m<sup>2</sup> =  $5.0 \times 10^{-7}$  m<sup>2</sup>.

$$\epsilon_c = \frac{2G_c h^e}{\sigma_c A^e} = \frac{2(2578 \text{ J/m}^2)(0.001 \text{ m})}{(100 \text{ MPa})(5.0 \times 10^{-7} \text{ m}^2)} \approx 0.1 \quad (2)$$

In order to understand the effects of the critical crack opening stretch on fracture morphology, the critical crack opening stretch was varied between 0.1 and 0.001 m. Figure 3 shows mid-tibia compressive axial stress plotted in terms of compressive axial strain applied to the ends of the tibia for all three values of critical crack opening stretch examined. Once the crack opening critical stretch is attained the elements are deleted from the computation, thus the mass of the elements are also removed from the total system. In other words, the total mass of the system decreases as fracture increases. Using this information, a simplistic damage parameter,  $D$ , can be defined as:

$$D(t) = 1 - \left( \frac{M_{current}(t)}{M_{initial}} \right) \quad (3)$$

where  $M_{current}(t)$  is the mass of the system at time  $t$ , and  $M_{initial}$  is the mass of the system at  $t = 0$ . The damage defined here ranges between 0 and 1, with 1 representing the fully damaged system. Damage versus time is also plotted in Figure 3.

After initial compressive loading, stress softening occurs at 0.2% strain, roughly between 150–300  $\mu$ s. Note at this time the damage parameter also begins to grow indicating crack initiation. Stress values for the initial softening peak are similar for all three critical crack opening stretch values, implying that the fracture initiation is similar. However, secondary stress softening that occurs between 0.4 and 0.6% compressive strain are as much as 26% different, with noticeably significant values for damage. This stress increase and then softening continues during the failure process. The maximum peak compressive axial stress reached is approximately 190 MPa, 180 MPa and 160 MPa for critical crack opening stretch values of 0.1, 0.01 and 0.001, respectively. These stresses correspond to nominal axial forces of approximately 41.4 kPa, 39.2 kPa and 34.8 kPa, respectively. The rate of damage growth is faster for smaller values of critical stretch which prevent the tibia structure to support load for more applied strain or longer duration leading to higher peak loads obtained.

Figure 4 shows fracture profiles for all three values of critical crack opening stretch. Time snapshots of the failure process is also shown. For the case of  $\epsilon_c = 0.001$  shown in Figure 4(a) fracture initiates approximately 0.483 ms, however that fracture is near the location of applied boundary conditions. At 1.861 ms Figure 4(a) shows how the fracture has initiated near the mid-tibia where the cross sectional area is minimum. There are three microcracks in the process of propagation. At 2.344 ms more microcracks are initiated and are propagating, and some microcracks have coalesced with others. At 3.335 ms almost complete coalescence has

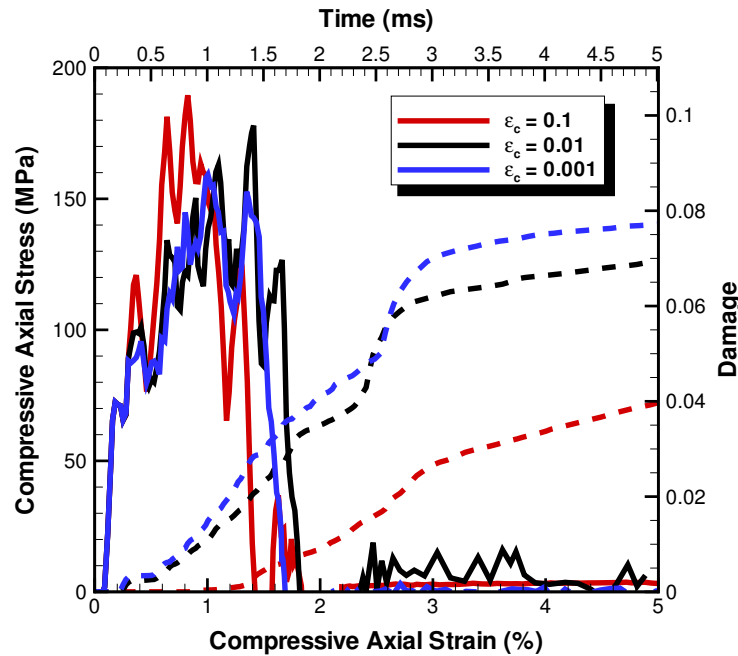


Figure 3: Compressive axial stress (solid) and damage (dashed) plotted in terms of axial compressive strain and time, respectively, for various critical crack opening stretch values.

occurred indicated by the fragments of bone isolated in space. At 4.596 ms the bone is completely fractured and is not capable of carrying any load due to the fragmentation.

A similar process occurs for larger values of  $\epsilon_c$ , however since the critical stretch is larger crack growth is limited which thus decreases the number of fragments and also increases fragment size.

### 2.2.2 Effect of Strain Rate

One long-term goal of this research is to accurately predict the fracture morphologies of the bones within the lower extremities as a function of various extrinsic factors such as loading rate, especially since the mechanical properties of bone have been reported to be strain rate dependent. Hansen *et al.* [16] measured the properties of human femoral cortical bone at strain rates ranging between  $0.14 - 29.1 \text{ s}^{-1}$  in compression and  $0.08 - 17 \text{ s}^{-1}$  in tension. They found that Young's modulus generally increased, across this strain rate range, for both tension and compression.

Figure 5 shows the compressive axial stress versus time for some of the strain rates investigated including  $10, 25$  and  $50 \text{ s}^{-1}$ . The strengthening observed in these simulations is similar to that observed in experiments on other brittle materials and is believed to be primarily a result of inertial effects. Unlike some micro-mechanical models, inertial effects are not supplied to the constitutive description (*e.g.* through crack growth dynamics laws) in these simulations. Instead, dilatation of the highly damaged specimens is suppressed because material fragments (which have mass) resist motion. At high strain rates rapid nucleation and coalescence of many cracks is a result of large stresses that develop in the specimen due to the high rate-of-deformation.

As shown in Figure 6, the damage as defined by Equation 3 has an increased rate of growth as strain rate increases. The total amount of damage also increases with increasing strain rate. Also shown in the figure

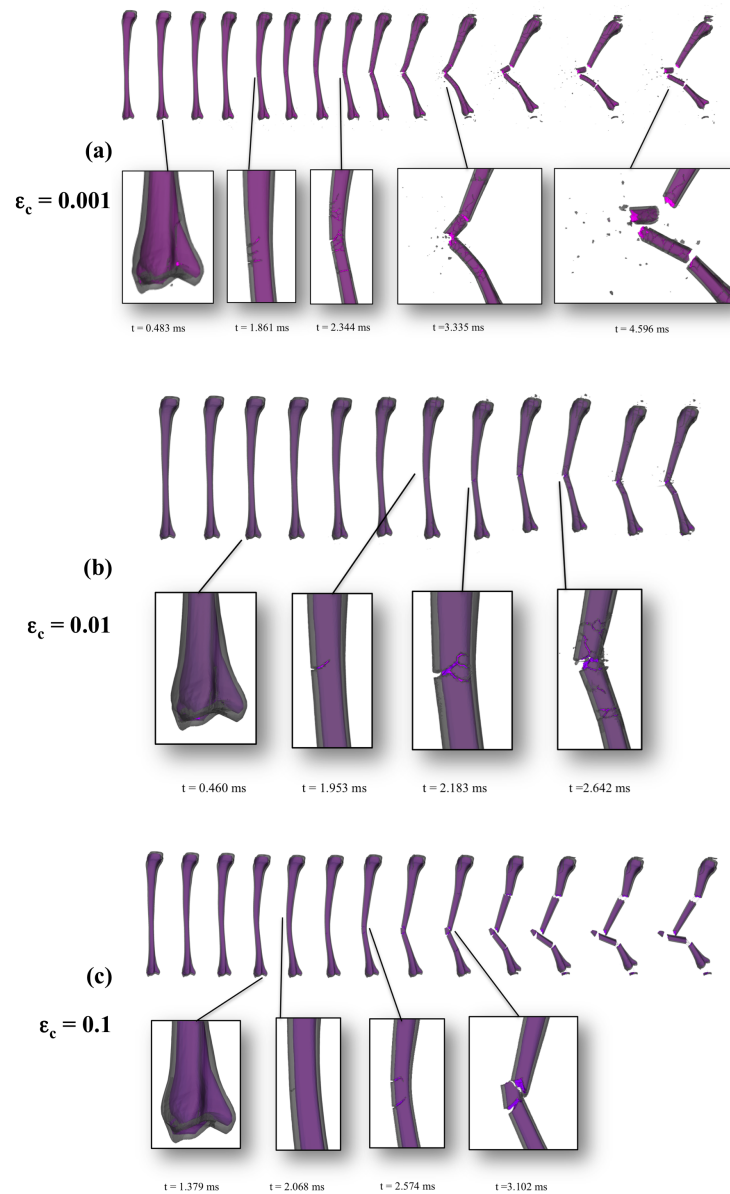


Figure 4: Compressive failure response for the tibia subjected to compressive loading at a nominal strain rate of  $10 \text{ s}^{-1}$  using a critical crack opening stretch of (a) 0.001, (b) 0.01 and (c) 0.1.

are snapshots of the fragmentation for the lowest and highest strain rate. It is apparent from the damage-time curves that crack initiation occurs much sooner for higher rates of loading, however cracks initiate in very different spatial locations. For lower rates, fracture morphology appears to more transverse near the mid-tibia whereas for higher strain rates fracture seems to more proximal and could possibly more described as a pilon fracture. The transition for transverse fracture to comminution should be examined further to gain improved understanding of the effects of bone fragment size as a function of strain rate. From qualitative observations, it

appears that perhaps the general trend is that as the strain rate increases the fragments become smaller. In this model, the smallest allowable fragment size is the elements. Note that the decrease of fragment size with  $\dot{\epsilon}$  is also predicted by a number of theoretical and computational methods for compressive fragmentation [17].

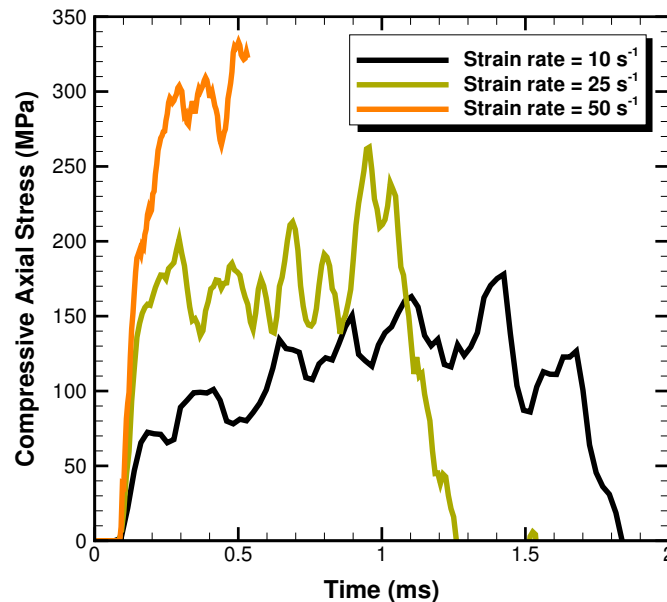


Figure 5: Compressive axial stress versus time for strain rates of 10, 25 and 50 s<sup>-1</sup>.

### 2.3 Modeling the Lower Leg Assembly

In accordance with our hierarchical validation and verification strategy presented in Section 2.1, we further consider one assembly within the full lower extremity model the lower leg of the region below the knee. Similar models have been used to simulate axial impulsive loading applied at the plantar surface of the foot in order to understand the dynamic response of the ankle related to injury [18]. Following Bandak *et al.* [18] the model in this study involves the simulation of cadaveric lower extremities under impulsive axial impact that attempt to mimic the experiments of Yoganandan *et al.* [19, 20]. In these experiments, human cadaveric lower legs with the ankle initially in the neutral position were impacted by a 24.5 kg pendulum at various initial velocities ranging from 2.23 m/s to 7.59 m/s [19, 20]. A similar model for the lower leg assembly was developed for this effort. Figure 7a shows the finite element model of the lower leg assembly. Figure 7b shows a schematic of the computational set-up corresponding to the experimental model.

For the lower leg assembly model, anatomy distal (below) the knee is represented. Bones, ligaments, muscles and skin are explicitly represented and fully-segmented, *i.e.* each bone, muscle, ligament, *etc.* can be assigned its own material properties. There are some geometry simplifications that were taken to help aid the model building process. In reality, bone consists of many layers and include cortical and trabecular components, plus medullary cavities in long bones. The model used in this study treats bone as an isotropic solid, homogenous body. In reality the foot bone structure consists of 26 bones, with numerous articulations and

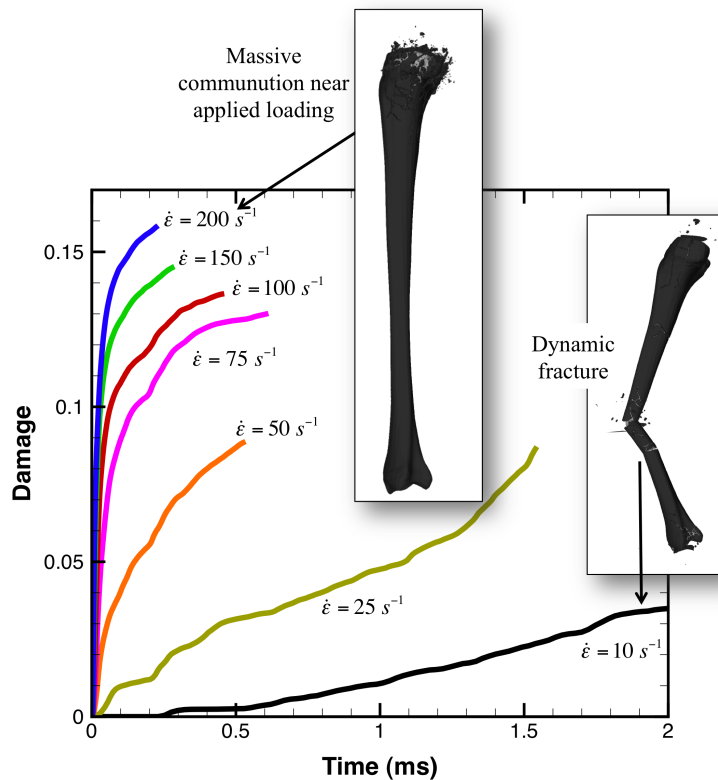


Figure 6: Damage versus time for various strain rates.

ligaments. The model used in this study uses a shrink-wrapped mid- and forefoot (the talus, navicular, cuboid, cuneiforms, metatarsals, and phalanges are fused). The calcaneus was not altered so the foot is represented as two objects: “forefoot” and calcaneus. In reality, 13 muscles run along the tibia and fibula in the lower leg. In the model only 4 of those muscles are explicitly represented currently; the tibialis anterior, tibialis posterior, flexor hallucis longus and peroneus brevis. Tendons are not identified or separated from muscle bodies. For the other soft tissues, a bulk material was utilized to encompass the remaining muscles, ligaments, *etc.* For example, for the ankle joints gaps between bones were filled in with the bulk material. Articular cartilage, joint capsules, synovial fluid, bursa, *etc.*, are not explicitly represented. All components of the model (bones, muscles, ligaments, skin) share nodes at their interfaces *i.e.* are tied together. Finally, a rectangular plate was developed and placed directly underneath and in contact with the skin of the foot. This plate represented the floor of the truck where the blast would occur beneath. During the simulations, all forces affecting the leg model would first travel through this plate.

Two versions of the lower leg model with different bone mesh densities (coarse and fine) were developed in this study. A comparison between the two can be visualized in Figure 8. For the coarse mesh, there were a total of 543,386 elements in the model which includes 44,180 elements for the tibia, 29,540 elements for the fibula, 32,522 elements for the foot and 5,713 elements for the calcaneus. For the fine mesh, there were a total of 5,302,920 elements in the model which includes 543,351 elements for the tibia, 285,199 elements for the fibula, 83,233 elements for the foot and 54,370 elements for the calcaneus. The simulations of the lower leg discussed in this paper were performed on the coarse bone mesh model. The fine mesh model will be used for

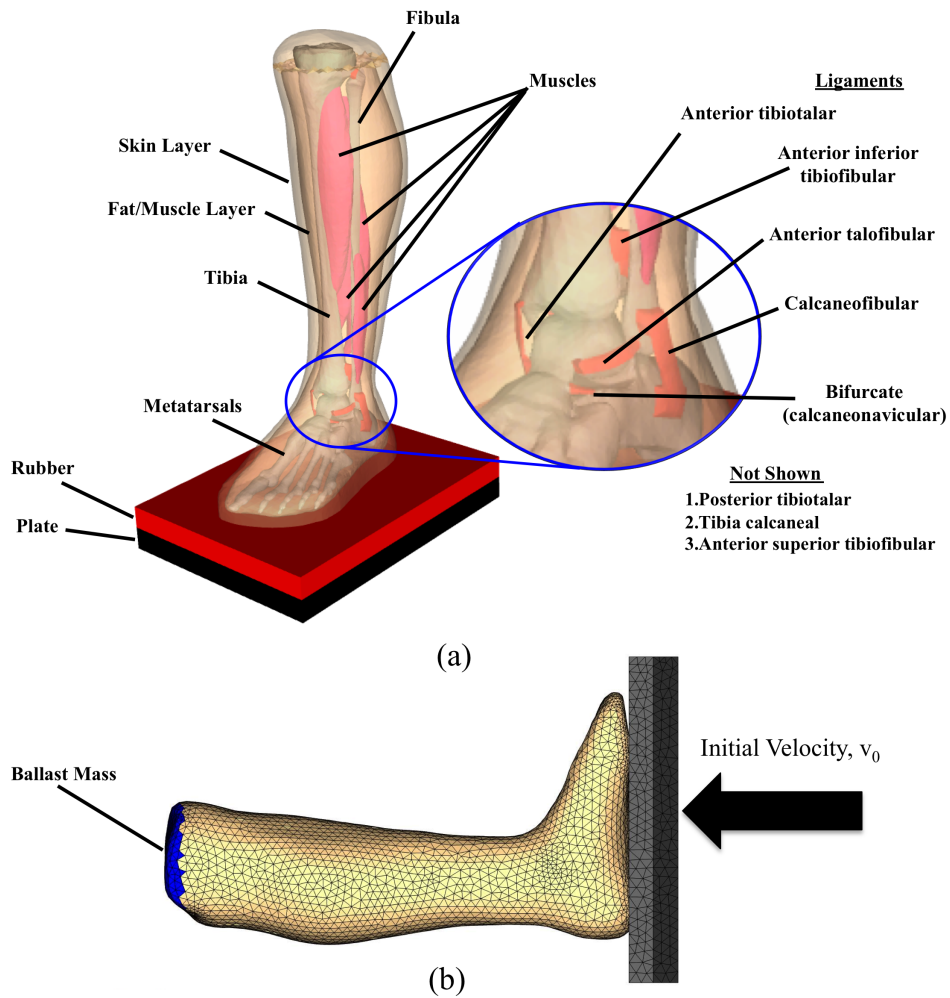


Figure 7: (a) Lower leg model geometry, and (b) applied velocity.

future study for better visualization of crack growth and propagation. Similar to Bandak *et al.* [18], an initial velocity was applied to the rubber-plate impactor. In this study,  $v_o = 10$  m/s. A ballast mass of 11.3 kg at the top (proximal) end of the tibia was used in accordance with Bandak *et al.* [18] to simulate the weight of the experimental slider used by Yoganandan *et al.* [19, 20].

Table 1 gives a list of the material constitutive models and parameters used in this study. Skeletal muscle tissue has been shown to exhibit non-linear anisotropic viscoelastic behavior across many strain rate loading regimes. In this model, the tissue is treated as non-linear viscoelastic using a viscoelastic Swanson model where the bulk response is elastic and the deviatoric response is viscoelastic [21, 22]. The non-linear elastic properties are obtained from the recent work of Lu *et al.* who represented skeletal muscle tissue as a composite of an isotropic ground substance and muscle fibers [23]. The isotropic matrix was modeled using a hyperelastic neo-hookean constitutive law. We neglect the anisotropic muscle fiber contribution at this time. Van Looke *et al.* examined the viscoelastic properties of passive skeletal muscle in compression [24].

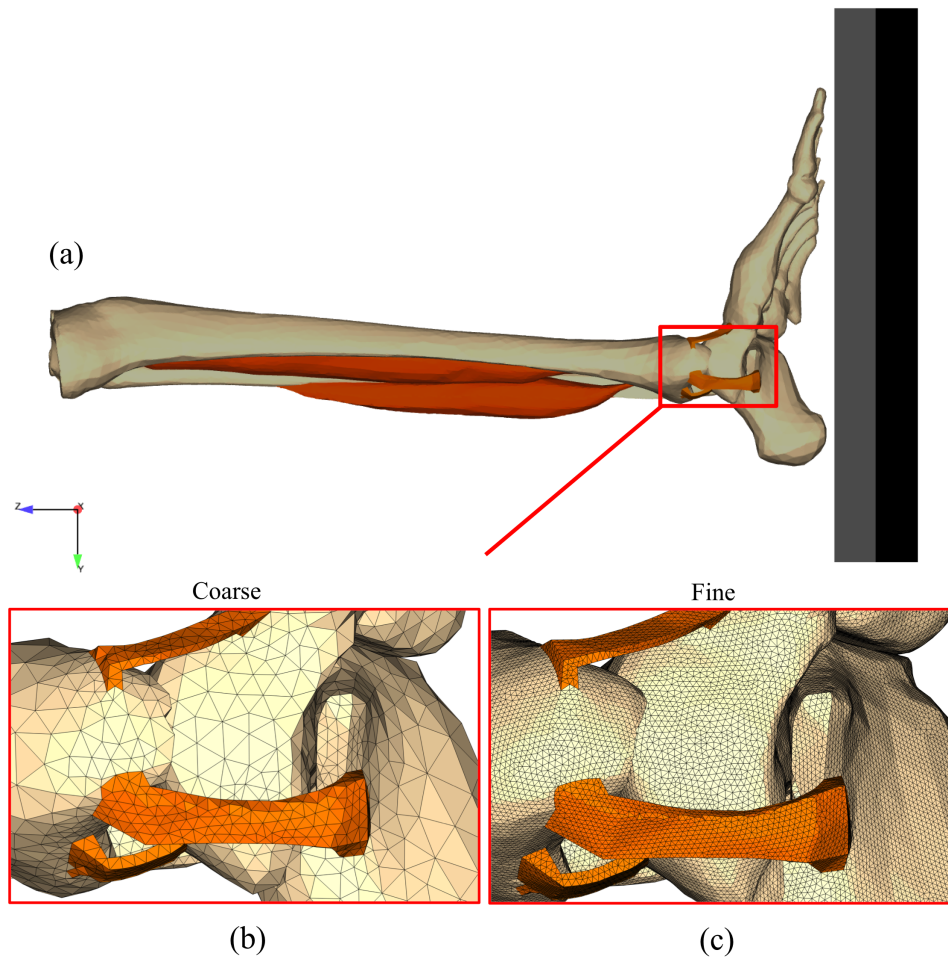


Figure 8: Mesh of the ankle complex within the lower leg assembly model.

Figure 9 shows that some degree of load sharing occurs between the tibia and fibula when the lower leg is loaded axially. This is consistent with real-life behavior of the lower leg, and is a result unique to simulations of actual human anatomy (the Hybrid-III surrogate and its corresponding finite element models do not have a fibula). In the time series contours, it can be seen that the forefoot experiences the majority of load resulting in significant material failure and element deletion. This is most likely an artifact of the simplified geometry used where the entire forefoot was rigid; none of the articulations between the metatarsals, tarsals, and phalanges were represented in this model. Furthermore in Figure 9, it can be seen that the calcaneus pivots around what would be the ankle joint (displacements are magnified by a factor of 2 in the figure). This suggests that the area representing the ankle joint in this model must be stiffened to prevent this rotation of the calcaneus such that crushing fracture on the planter surface of the heel can be observed, as that is a common injury experienced in vehicular underbelly blasts that should be captured.

**Table 1: Compilation of various constitutive models and parameters used for the lower leg simulation. E is the Young's Modulus,  $\nu$  is Poisson's ratio,  $\sigma_c$  is the critical failure stress,  $\epsilon_c$  is the critical crack opening stretch,  $g_\infty$  is the long-term shear modulus,  $g_n$  are prony series shear terms,  $\rho$  is the density and K is the bulk modulus.**

Anatomic Component	Material Model	Material Properties	References
Bone	Cortical bone	Elastic with maximum principle stress-based fracture model E = 22.27 GPa $\nu = 0.3$ $\sigma_c = 150$ MPa $\epsilon_c = 0.1$ $\rho = 1810$ kg/m <sup>3</sup>	[15]
	Trabecular bone	Elastic with maximum principle stress-based fracture model E = 300 MPa $\nu = 0.45$ $\sigma_c = 132$ MPa $\epsilon_c = 0.1$ $\rho = 600$ kg/m <sup>3</sup>	[25]
Muscles/Ligaments	Isotropic Visco-Hyperelastic (Mooney-Rivlin)	K = 167 MPa C <sub>10</sub> = 0.94 MPa <sup>-1</sup> C <sub>01</sub> = 0.94 MPa $g_\infty = 0.123$	[23, 26]
		$g_1 = 0.465, \tau_1 = 0.6$ sec	[24]
		$g_2 = 0.2, \tau_2 = 6.0$ sec	[24]
		$g_3 = 0.057, \tau_3 = 30.0$ sec	[24]
		$g_4 = 0.066, \tau_4 = 60.0$ sec	[24]
		$g_5 = 0.089, \tau_5 = 300.0$ sec $\rho = 1000$ kg/m <sup>3</sup>	[24]
Rubber Shoe Sole	Elastic	E = 1 GPa $\nu = 0.4$	

## 2.4 Real World Physical System

In order to establish a system of models ranging from individual components to the full real world system, simplifications were made. For the full lower extremity model, simple geometry consisting of cylinders for the bones and surrounding muscle, hexahedral shapes for the foot and non-friction contact interfaces for the joints were used to obtain a qualitative response force-time curve for underbelly loading. Due to the lack of anatomic geometry, and robust constitutive models and parameters, this approach is useful to understand the macroscopic impact kinematics, but of little use for understanding specific injury mechanisms. Similar to the computational study of Nilakantan and Tabiei [2] a plate which represents the vehicle floor plate, reaches a vertical velocity of 10.7 m/s after 5 ms. While Nilakantan and Tabiei used a computational model of a Hybrid-III surrogate, here we use more realistic material properties for bone and soft tissue.

As shown in Figure 10, within approximately 2 ms of loading the axial compressive force in the mid-tibia is attained, followed by a sharp rate of change in the force-time response - a so-called force "plateau". This force "plateau" is due to the fact that the velocity of the tibia has reached a constant value because the upper leg (between the knee and the pelvis) has begun to travel at near constant velocity. The applied loading to the floor plate ends at 5 ms at which time the force response diminishes to zero. Figure 10 shows results of this simplified model compared to the dynamic tibia response for Hybrid-III human surrogates [2] and cadaveric experiments [27] using similar boundary conditions.

When including muscle components into the skeletal model, the materials shear modulus became an important contributor to the axial compressive force inflicted on the tibia. These experiments showed that the shear

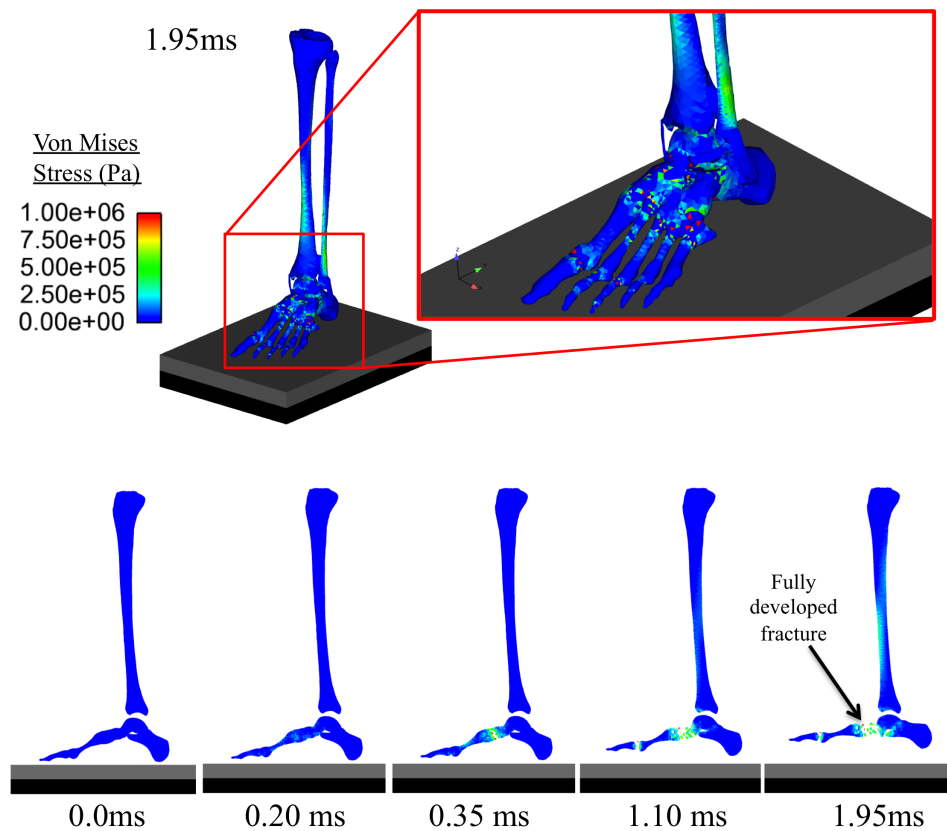


Figure 9: Simulation contours of the lower leg (course model) subjected to vertical loading process of  $10 \text{ s}^{-1}$ .

modulus within the muscle could control behavior within the initial 1 ms of the tibial injury event. As shown in Figure 11 high shear modulus for muscle was made an upper bound by making it 26.8 MPa. Low shear modulus was controlled by a lower bound of 26.8 kPa. The magnitude of compressive force within this time frame was maximal, around 2000 N, when the muscle exhibited high shear properties. When the muscle exhibited low shear muscle, or no muscle at all, the force was half as much as its high shear counterpart. It was found that this correlation was indirectly related to the muscles effect on rate of accelerative loading. High-shear muscle led to a slower rate of tibial acceleration, due to the muscle's inertial effects. The low-shear and no muscle's rate of acceleration was nearly three times that of high-shear muscle. This result shows that there is a clear link between rate of accelerative loading and compressive force levels within the tibia.

While this approach fails to give insight into the mechanics of any specific lower extremity injury, it does provide insight into the bio-kinematics of the lower extremities during an explosive event. The approach was also very useful to understand the importance of the contributions of individual components such as the muscle or joints to the overall real world physical system model. In addition, a simplified model that offers macroscopic results quickly, such as this, could be use to develop boundary conditions for the smaller length scale models including assemblies and subassemblies. For example, it is important to note that the mid-tibia axial force reaches a maximum value within 2 ms of loading.

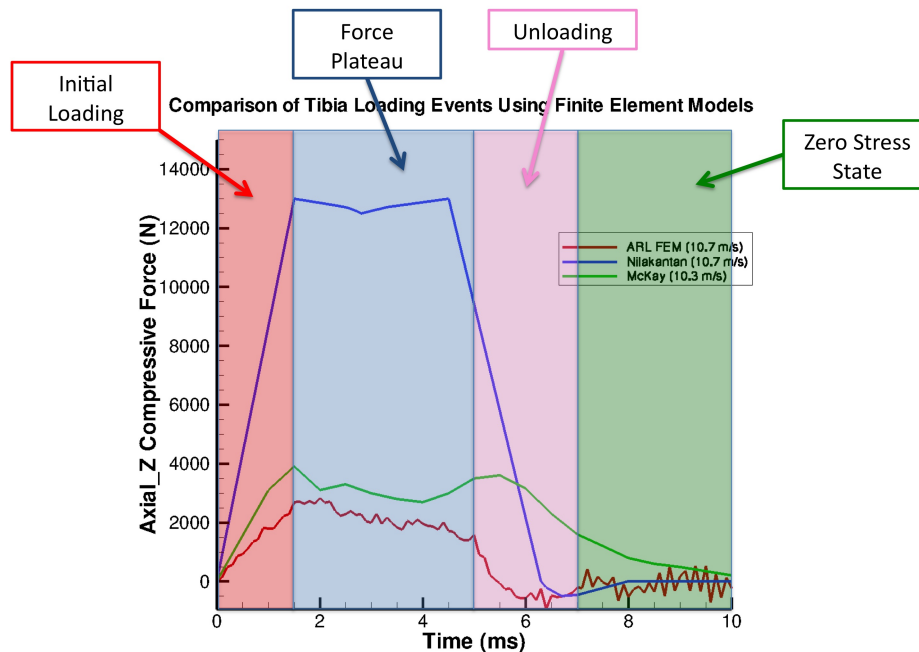


Figure 10: For the full lower extremity model, simple geometry consisting of cylinders for the bones and surrounding muscle, hexahedral shapes for the foot and non-friction contact interfaces for the joints were used to obtain a qualitative response force-time curve for underbelly loading. Results are compared to simulations of Hybrid-III surrogates [2] and cadaveric experiments [27].

### 3.0 CONCLUSIONS AND FUTURE WORK

This paper has described a research effort to develop a hierarchical modeling approach for the lower extremities subjected to military underbelly blasts and has specifically focused on developing a finite element model of the lower extremities undergoing high strain rate blast-induced deformation. At the component level, the process of bone fracture and fragmentation from high strain rate axial loading to the tibia was investigated. The effect of critical crack opening stretch and strain on the resulting leg fracture was studied and had significant influence on fracture morphology. Apparent strengthening was observed for higher rates of loading, which are attributed to inertial effects. At the assembly level, a lower leg consisting of many different tissues was developed and evaluated. Similar to past experimental research, we numerically observe calcaneal, talar, midfoot fractures, as well as ankle rotation before any tibia or fibula fracture is observed. At the system (full lower extremity) level, simulations consisting of simplified geometry with more realistic material constitutive laws as compared to Hybrid III finite element models were developed. The models captured the kinematics of the lower leg and the axial tibia force was compared to cadaveric experimental tests as well as results from a Hybrid III human surrogate finite element model. All three models need to be studied in more depth and refined. For example, for each component within the lower leg assembly a computational model should be developed and analyzed - both computationally and experimentally. To summarize, the following offers a list of future work that should be completed:

- Experimental and computational component level studies including bone, ligaments, muscle and skin at

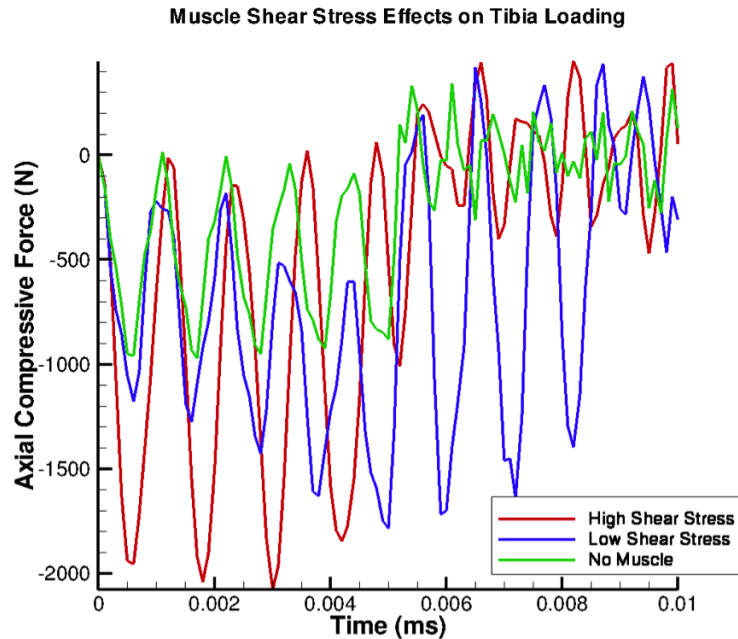


Figure 11: Effect of soft tissue shear modulus on the axial compressive force.

the appropriate strain rates.

- Include more complex material models using anisotropic and poro-visco-elasticity that capture the realistic tissue response.
- Examine additional assemblies, such as the knee-thigh-pelvis complex.
- Develop computational model of lower extremities that is linked with the spine to elucidate injury mechanism associated with coupled loading.
- Improve the computational scalability and performance on supercomputing resources.
- Improve availability of human data pertaining to lower leg impact during a mine blast underneath armored vehicles, especially testing on human cadavers in order to better understand the injury assessment and establish a reliable and extensive source of data.
- Leverage detailed understanding of injury criteria obtained from computational studies to further refine military blast injury criteria.
- Use injury mechanism-based understanding to improve protection system design.

In conclusion, computational failure modeling of the lower extremities offers valuable opportunities to improve protection for the Warfighter.

## ACKNOWLEDGMENTS

Thanks to all who helped and for this template [28].

**REFERENCES**

- [1] Whitlock, C., “Soaring IED Attacks in Afghanistan Stymie U.S. Counteroffensive,” March 2010, [Online; accessed 13-August-2010].
- [2] Nilakantan, G. and Tabiei, A., “Computational Assessment of Occupant Injury Caused by Mine Blasts underneath Infantry Vehicles,” *International Journal of Vehicle Structures & Systems*, Vol. 1, No. 1–3, 2009, pp. 50–58.
- [3] Gabauer, D. J. and Gabler, H. C., “Acceleration-Based Occupant Injury Criteria For Predicting Injury In Real-World Crashes,” *Biomedical Sciences Instrumentation*, Vol. 44, 2008, pp. 219–218.
- [4] Department of Defense, “DoD Directive 6025.21E: Medical Research for Prevention, Mitigation, and Treatment of Blast Injuries,” Electronic Documentation, 2006.
- [5] Ramasamy, A., Hill, A. M., Hepper, A. E., Bull, A. M. J., and Clasper, J. C., “Blast Mines: Physics, Injury Mechanisms and Vehicle Protection,” *Journal of the Royal Army Medical Corps*, Vol. 155, No. 4, 2009, pp. 258–264.
- [6] 25, N. H.-. T. G., “Test Methodology for Protection of Vehicle Occupants against Anti-Vehicular Landmine Effects,” Tech. Rep. RTO-TR-HFM-090, NATO Research and Technology Organization, 2007.
- [7] Kuppa, S., Wang, J., Haffner, M., and Eppinger, R., “Lower extremity injuries and associated injury criteria,” *Proceedings of the 17th International Technical Conference on the Enhanced Safety of Vehicles*, National Highway Traffic Safety Administration, Washington, DC, 2001., Paper Number: 457.
- [8] Manning, P., Wallace, A., Owen, C., Roberts, A., Oakley, C., and Lowne, R., “Dynamic Response and Injury Mechanism in the Human Foot and Ankle and an Analysis of Dummy Biofidelity,” *Proceedings of the 16th International Conference on Enhanced Safety of Vehicles*, Canada, June 1998., pp. 1960–1998, Paper No.: 98-S9-O-11.
- [9] Crandall, J. R., Kuppa, S. M., Klopp, G. S., Hall, G. W., Pilkey, W. D., and Hurwitz, S. R., “Mechanisms of injury and injury criteria for the human foot and ankle in dynamic axial impacts to the foot,” *International Journal of Crashworthiness*, Vol. 3, No. 2, 2003, pp. 147–162.
- [10] Begeman, P. and Paravasthu, N., “Static and dynamic compression loading of the lower leg,” *Proceedings of the 7th Injury Prevention Through Biomechanics Symposium*, Detroit, MI, 1997.
- [11] Manseau, J. and Keown, M., “Development of an Assessment Methodology For Lower Leg Injuries Resulting from Anti-Vehicular Blast Landmines,” *IUTAM Symposium on Impact Biomechanics: From Fundamental Insights to Applications*, edited by M. D. Gilchrist, Vol. 124, Springer, The Netherlands, 2005, pp. 33 –40.
- [12] Belytschko, T., Liu, W. K., and Moran, B., *Nonlinear Finite Elements for Continua and Structures*, John Wiley & Sons, LTD., New York, 2000.
- [13] Thacker, B. H., Francis, W. L., and Nicolella, D. P., “Model Validation and Uncertainty Quantification Applied to Cervical Spine Injury Assessment,” *Computational Uncertainty in Military Vehicle Design (pp. 26-1 26-30). Meeting Proceedings RTO-MP-AVT-147, Paper 26*, Neuilly-sur-Seine, France: RTO, 2007.

- [14] Song, J.-H., Wang, H., and Belytschko, T., “A comparative study on finite element methods for dynamic fracture,” *Computational Mechanics*, Vol. 42, 2008, pp. 239–250, 10.1007/s00466-007-0210-x.
- [15] Ural, A., Zioupos, P., Buchanan, D., and Vashishth, D., “The effect of strain rate on fracture toughness of human cortical bone: A finite element study,” *Journal of the Mechanical Behavior of Biomedical Materials*, Vol. In Press, Corrected Proof, 2011, pp. –.
- [16] Hansen, U., Zioupos, P., Simpson, R., Currey, J. D., and Hynd, D., “The Effect of Strain Rate on the Mechanical Properties of Human Cortical Bone,” *Journal of Biomechanical Engineering*, Vol. 130, No. 1, 2008, pp. 011011.
- [17] Kraft, R., Molinari, J., Ramesh, K., and Warner, D., “Computational micromechanics of dynamic compressive loading of a brittle polycrystalline material using a distribution of grain boundary properties,” *Journal of the Mechanics and Physics of Solids*, Vol. 56, No. 8, 2008, pp. 2618 – 2641.
- [18] Bandak, F. A., Tannous, R. E., and Toridis, T., “On the development of an osseo-ligamentous finite element model of the human ankle joint,” *International Journal of Solids and Structures*, Vol. 38, No. 10-13, 2001, pp. 1681 – 1697.
- [19] Yoganandan, N., Pintar, F., Boyton, M., and Sances, J. A., “Biomechanics of foot and ankle fractures,” *In the Proceedings of the International Conference on Pelvic and Lower Extremity Injuries*, 1995, pp. 201–209.
- [20] Yoganandan, N., Pintar, F., Boyton, M., Begeman, P., and Prasad, P., “Dynamic axial tolerance of the human foot-ankle complex,” *In the Proceedings of 40th Stapp Car Crash Conference*, 1996, pp. 207–218.
- [21] Swanson, S. R. and Christensen, L. W., “A constitutive formulation for high-elongation propellants,” *Journal of Spacecraft and Rockets*, Vol. 20, No. 6, 1983, pp. 559–566.
- [22] Scherzinger, W. M. and Hammerand, D. C., “Constitutive Models in LAME,” Tech. Rep. SAND2007-5873, Sandia National Laboratory, 2007.
- [23] Lu, Y., Zhu, H., Richmond, S., and Middleton, J., “A visco-hyperelastic model for skeletal muscle tissue under high strain rates,” *Journal of Biomechanics*, Vol. 43, No. 13, 2010, pp. 2629 – 2632.
- [24] Loocke, M. V., Lyons, C., and Simms, C., “Viscoelastic properties of passive skeletal muscle in compression: Stress-relaxation behaviour and constitutive modelling,” *Journal of Biomechanics*, Vol. 41, No. 7, 2008, pp. 1555 – 1566.
- [25] Schuster, P. J., Chou, C. C., Prasad, P., and Jayaraman, G., “Development and Validation of a Pedestrian Lower Limb Non-Linear 3-D Finite Element Model,” *Stapp Car Crash Journal*, Vol. 44, 2000, pp. 215–334.
- [26] Chawla, A., Mukherjee, S., and Karthikeyan, B., “Characterization of human passive muscles for impact loads using genetic algorithm and inverse finite element methods,” *Biomechanics and Modeling in Mechanobiology*, Vol. 8, 2009, pp. 67–76, 10.1007/s10237-008-0121-6.
- [27] McKay, B. J., *Development Of Lower Extremity Injury Criteria And Biomechanical Surrogate To Evaluate Military Vehicle Occupant Injury During An Explosive Blast Event*, Ph.D. thesis, Wayne State University, 2010.

- [28] Kleb, B., “nato-rto—A  $\text{\LaTeX}$  Class and  $\text{\BibTeX}$  Style for NATO-RTO Meeting Proceedings Papers (MPs) and Educational Notes (ENs),” Electronic Documentation, Sept. 2007, Version 1.2.2.